Metal–organic framework/graphene oxide composites for CO 2 capture by microwave swing adsorption

Mégane Muschi, Sabine Devautour-Vinot, Damien Aureau, Nicolas Heymans, Saad Sene, Rudolf Emmerich, Alexandros Ploumistos, Amine Geneste, Nathalie Steunou, Gilles Patriarche, et al.

Metal-Organic Framework/Graphene Oxide composites for CO_2 Capture by Microwave Swing Adsorption

Mégane Muschi[a], Sabine Devautour-Vinot[b], Damien Aureau[c], Nicolas Heymans[d], Saad Sene[a], Rudolf Emmerich[e], Alexandros Ploumistos[a], Amine Geneste[b], Nathalie Steunou[a,c], Gilles Patriarche[f], Guy De Weireld[d], Christian Serre*[a]

a. Institut des Matériaux Poreux de Paris, ESPCI Paris, Ecole Normale Supérieure, CNRS, PSL University, 75005 Paris, France.
   Email : christian.serre@espci.psl.eu
b. ICGM, Univ. Montpellier, CNRS, ENSCM, Montpellier, France.
c. Institut Lavoisier de Versailles, UMR 8180 CNRS, Université de Versailles St Quentin en Yvelines, Université Paris Saclay, Versailles, France.
d. Service de Thermodynamique et de Physique mathématique, Faculté Polytechnique, Université de Mons, 7000 Mons, Belgium.
e. Fraunhofer Institute for Chemical Technology ICT Joseph-von-Fraunhofer St. 7, 76327 Pfinztal, Germany.
f. Université Paris-Saclay, CNRS, Centre de Nanosciences et de Nanotechnologies, 91120, Palaiseau, France.

Abstract

Metal-organic frameworks (MOFs)/Graphene oxide (GO) composites are the subject of a growing interest due to their properties which can exceed those of the pure components, including post-combustion CO_2 capture. Series of composites suitable for CO_2 capture under flue gas conditions based on the microporous water stable MIL-91(Ti) have been prepared with different GO contents, following two routes, *in situ* and post-synthetic. It was observed that the *in situ* composite with 5wt% GO exhibits a semi-conducting behavior while the post-synthetic materials are insulating,

even with high (20wt%) GO content. As a consequence, this composite absorbs microwave radiations more efficiently compared to the pure MOF and post-synthetic materials. Finally, we report that CO_2 desorption is much faster under microwave irradiation compared to conventional heating on MOF/GO *in situ* materials, paving the way for future energy saving Microwave Swing Adsorption processes.

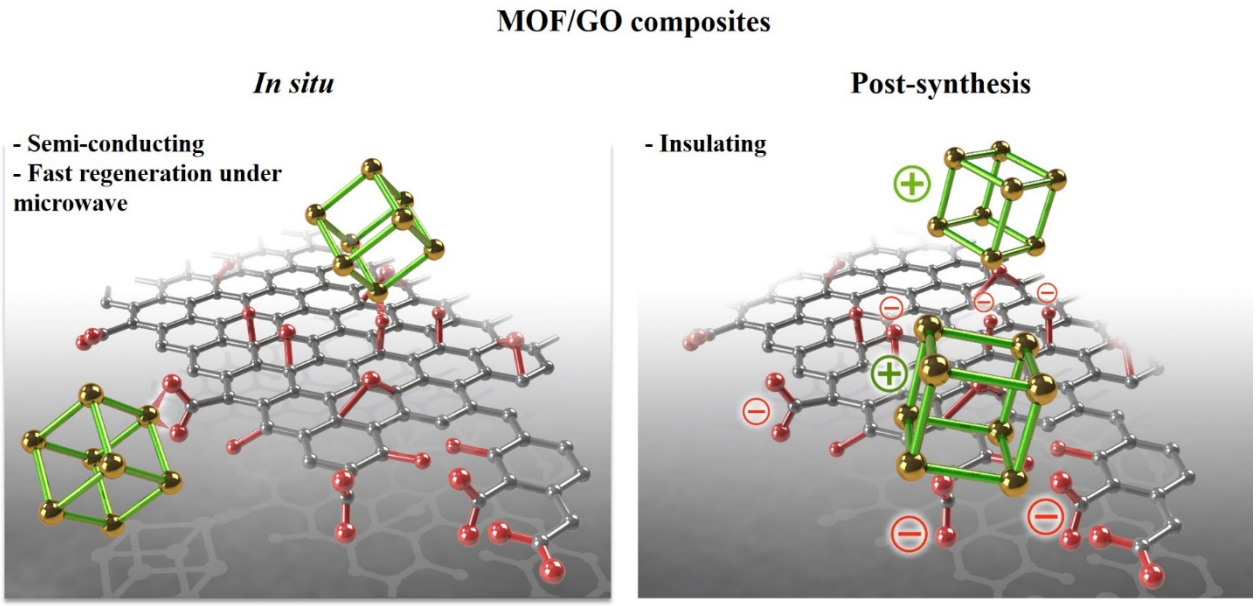

Introduction

Metal-organic frameworks (MOFs)/Graphene oxide (GO) composites have recently attracted a lot of attention due to the synergic effects between the two materials, leading to enhanced properties compared to the individual components.[1-3] It has for instance been shown that MOF/GO composites can exhibit higher porosity than the parent MOF and are suitable candidates for gas adsorption, including CO_2 capture.[4-7] In post-combustion industrial processes, the use of adsorbents usually involves pressure swing adsorption (PSA) or thermal swing adsorption (TSA) processes. The latter consists of heating the column during the desorption step to regenerate the material and should

allow for a lower energy penalty compared to other regeneration methods.[8, 9] However, it requires a homogeneous and fast heating rate of the material in the separation column. Unfortunately, MOFs exhibit very low thermal conductivities and the use of conventional heating is associated with slow desorption kinetics, which limits their practical use despite their suitable adsorption properties. Therefore, there is a need to find more efficient alternative desorption processes that would decrease the energy penalty related to the material regeneration. Among reported innovative desorption processes, the use of microwave irradiation, called microwave swing adsorption (MSA), has proven to lead to faster CO_2 release compared to conventional heating on solid adsorbents such as activated carbons.[10] Also, Lee *et al.* have shown that the use of microwave irradiation can be more efficient compared to conventional heating for MOF activation.[11] Therefore, these electromagnetic radiations should lead to faster CO_2 release compared to thermal or electrical heating, without damaging the adsorbent.

However, except from a few conductive 2D-MOFs that are not really suitable for CO_2 capture due to their lack of interactions with CO_2, their high cost and their poor hydrolytic stability,[12,13] MOFs usually exhibit very low electrical conductivity, associated with low dielectric losses and low microwave heating[14] that would hamper their use for MSA processes.

By combining them with graphene oxide or reduced graphene oxide, the electrical conductivity can however be significantly enhanced, which is of interest to develop new batteries, supercapacitors or address catalytic challenges[2] and for CO_2 capture through MSA process.

To date, several synthetic methods to prepare MOF/GO materials have been reported.[3] The most common routes are the *in situ* and the post-synthetic (*ex situ)* methods. The first one consists of mixing the MOF's precursors with GO prior to using the conditions required for the MOF

synthesis. In this case, some oxygenated groups of GO act as nucleation sites for the MOF, which leads to the formation of coordination bonds between these groups and the metal of the MOF.[15-17] The second method consists of mixing the pre-formed MOF particles with GO nanosheets, usually at a pH value at which the two materials exhibit oppositely charged surfaces to allow for electrostatic interactions. To our knowledge, only one study has compared these two types of composites in terms of microstructure and catalytic properties and has shown that they both strongly depend on the preparation route.[18] However, the electrical conductivity of these composites has never been compared. Recently, some of us have shown that the *in situ* formation of MIL-69(Al) in the presence of GO can lead to core-shell MIL-69(Al)-GO nanostructures. The peculiar microstructure of this composite strongly impacts their electron transport properties.[19]

Here, in order to develop suitable MOF/GO composites for CO_2 capture using MSA process, including a good CO_2 adsorption capacity and semi-conducting behavior, we report the synthesis by *in situ* and post-synthetic routes of new MOF/GO composites with different GO contents. The water stable MIL-91(Ti) that has already shown to be promising for post-combustion CO_2 capture has been selected.[20] We report first that *in situ* and post-synthetic materials exhibit significant differences in terms of electrical conductivity and microwave absorption properties, in relation with the composites' respective microstructures. Finally, we evidence the faster CO_2 desorption rate under microwave irradiation compared to conventional heating on microwave absorbing MOF/GO *in situ* composites based on MIL-91(Ti) and UiO-66-btc(Zr). We believe that *in situ* composites are therefore of strong interest for the future design of MSA based CO_2 capture processes (Figure 1).

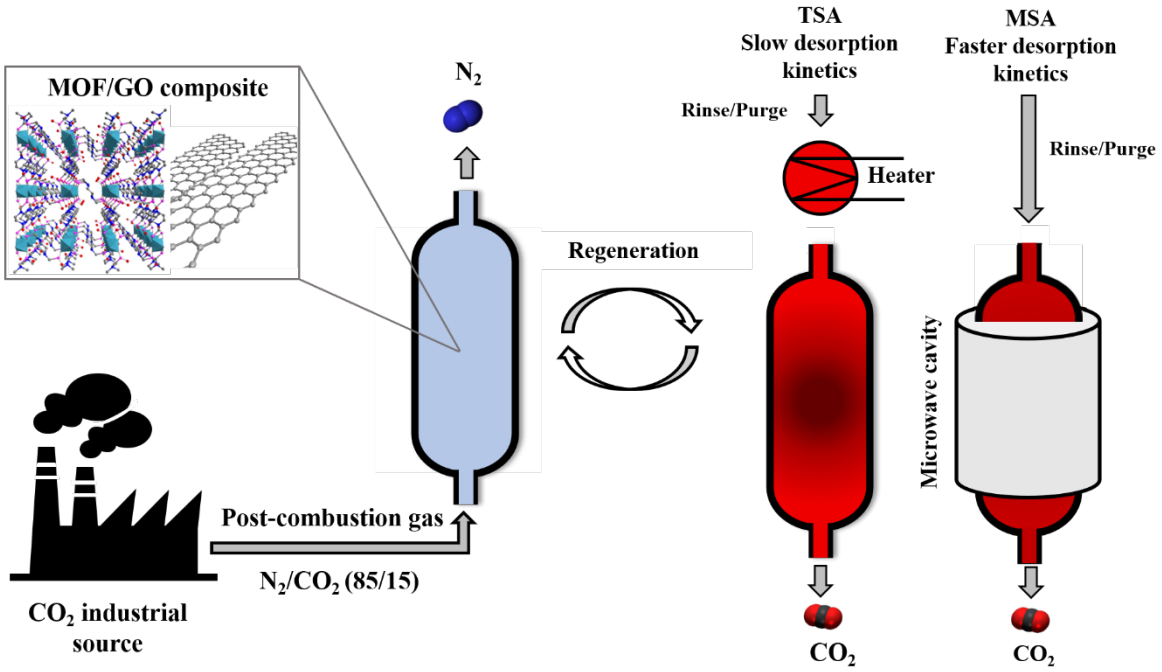

Figure 1. Schematic illustration of the MSA process compared to the TSA process on MOF/GO composites, illustrated with MIL-91(Ti)/GO, for CO_2 post-combustion capture.

Results and Discussion

Characterizations

MIL-91(Ti) is a microporous Ti(IV) phosphonate MOF made of corner-sharing chains of titanium octahedra connected by a bis-phosphonate linker delimiting narrow 1D pore channels (Figure 2).[21] This solid, together with its Al analogue MIL-91(Al), is a rare example of 3D metal phosphonate MOF that has shown promising results for post-combustion CO_2 capture with a high CO_2/N_2 selectivity and CO_2 adsorption capacity .[20] This hydrothermally stable material was synthesized using green conditions according to a modified literature procedure (Supporting information).[20]

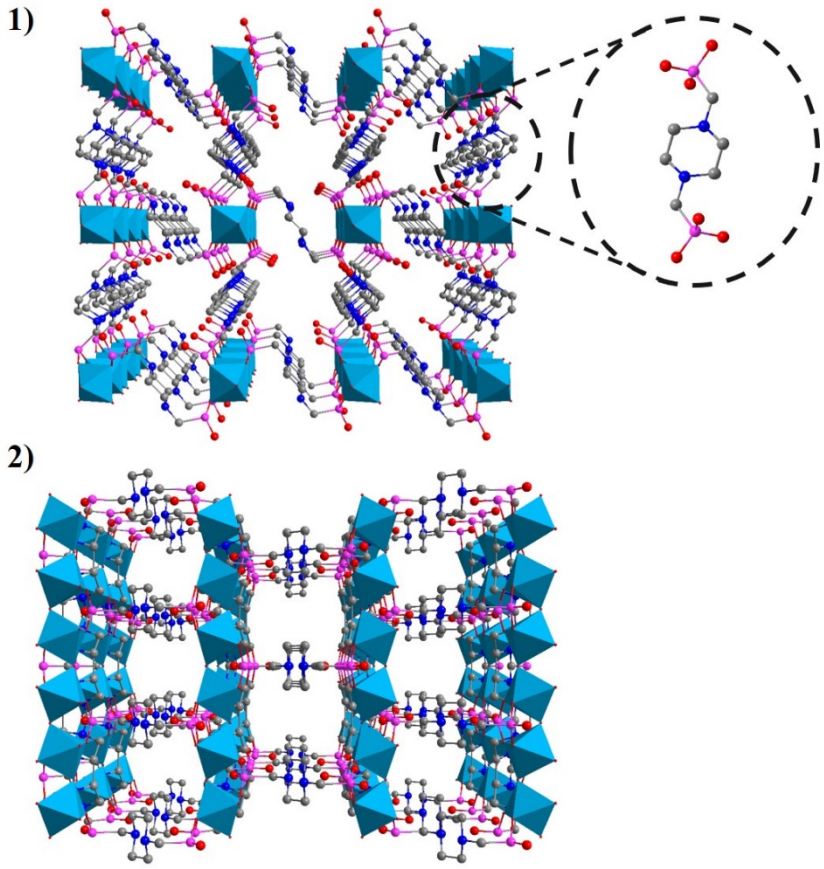

Figure 2. Crystal structure of MIL-91(Ti) along the 1) b axis with the structure of the linker 2) c axis. The titanium octahedra are represented in blue, the carbon, oxygen, nitrogen, phosphorus atoms in grey, red, dark blue and pink, respectively.

To optimize the sorption and physical properties of the composites for their use in CO_2 capture using MSA, *in situ* and post-synthesis MOF/GO materials were synthesized using variable amounts of GO (2-20 wt %). They will be denoted as MOF/GO*x*wt% where *x* is the theoretical mass of GO compared to that of the MOF.

To obtain the MIL-91(Ti)/GO post-synthesis composites, the zeta-potential of the pure components was first measured in deionized water to determine a pH range for which the two materials' surfaces (MOF, GO) are oppositely charged (Figure S4). Then, the MOF was dispersed in water and mixed

with a specific amount of GO at room temperature under a controlled pH value, close to 2.5, to lead to the self-assembly of the two materials through electrostatic interactions.

The preparation of MIL-91(Ti)/GO *in situ* composites was then investigated. Similar synthetic conditions as of the pure MOF were first considered, as reported for the synthesis of other MOF/GO *in situ* composites.[4, 5, 17, 22-28] The MOF' precursors were thus mixed with the GO nanosheets in water at room temperature prior to heating the mixture overnight under reflux. However, these conditions led to MOF/GO composites with a large amount of unreacted linker, suggesting a competition between the oxygenated groups of GO and the MOF linker to react with the metal species. Therefore, alternative synthetic conditions were investigated, consisting of adding the GO nanosheets dispersed in water to the reaction medium after the initial stage of the MOF's nucleation has begun, here after 6 hours under reflux. The reaction mixture was then left for an additional 16 hours under reflux (Supporting information).

The resulting composites were characterized by PXRD. As shown in Figure S5 the composites' patterns are similar to the one of the pure MIL-91(Ti), giving evidence of the successful *in situ* crystallization of the MOF. Note that the Bragg peak related to the [001] plane of pure GO, at 10.3°, is not observed for any of the composites. This suggests that for both types of composites, the long-range stacking of GO sheets is lost, in agreement with a disordered intercalation of some MOF's particles between the nanosheets. Also, for the *in situ* composites, the Bragg peaks width is slightly larger when increasing the GO content (Table S2). Although the particle size distribution is not narrow, this is in agreement with a decrease in particle size evidenced by TEM images (Figure S6). This decrease in size for the *in situ* materials with increasing the GO content has been attributed previously to the nucleation of the MOF on some oxygenated groups of GO, limiting the

growth of MOF particles related to the Ostwald ripening.[17, 29] It suggests that the *in situ* synthesis successfully led to the formation of coordination bonds between the metal of MIL-91(Ti) and some oxygenated groups of GO. This is in agreement with the higher thermal stability of the *in situ* composite compared to the post-synthetic one (Figure S7). In addition, when comparing the nitrogen porosimetry of the *in situ* composite with 5wt% GO with those of the pure MOF and post-synthetic composite with similar GO content, a higher BET surface area was obtained for the *in situ* material (Figure 3, Table 1). This is due to the creation of microporosity at the materials' interface, resulting from the coordination bonds between the two materials that maintain a close interface, as already discussed by Petit *et al*.[15] Those extra-micropores lead to a higher micropore area of the *in situ* composite compared to the two other materials (Table 1).

The effect of the GO content, between 2wt% and 20wt%, on the porosity was also studied by nitrogen porosimetry. As shown in Figure 3, the MIL-91(Ti)/GO2wt% *in situ* sample exhibits the highest BET surface area with 420 $m^2.g^{-1}$. With 5wt% GO, a slightly lower BET surface area of 400 $m^2.g^{-1}$ was obtained, which remains higher than that of the pure MOF (370 $m^2.g^{-1}$). When increasing the GO content up to 10 and 20wt% GO, a lower BET surface area of 230 $m^2.g^{-1}$ was however obtained. This decrease cannot be explained only by the presence of non-porous GO. Therefore, it suggests a partial pore blocking of the MOFs' channels by GO nanosheets, particularly when considering the very narrow pores of MIL-91(Ti). This was confirmed by the decrease of the accessible micropore area when increasing the GO content within the composite (Table S3). In addition, the adsorption isotherms show different shapes when the GO content increases, in agreement with an increase of the external surface area within the material (Table S3).

Note that to select the most appropriate composite for the MSA process, a compromise between the porosity and microwave absorption properties must be found. Indeed, as GO is the microwave absorber, its content within the composite must be high enough to efficiently lead to an increase of the temperature under microwave irradiation without using an excessive power. Therefore, despite the slightly higher BET surface area of the MIL-91/GO2wt% *in situ* composite, we selected the MIL-91/GO5wt% *in situ* material for the next steps of this study.

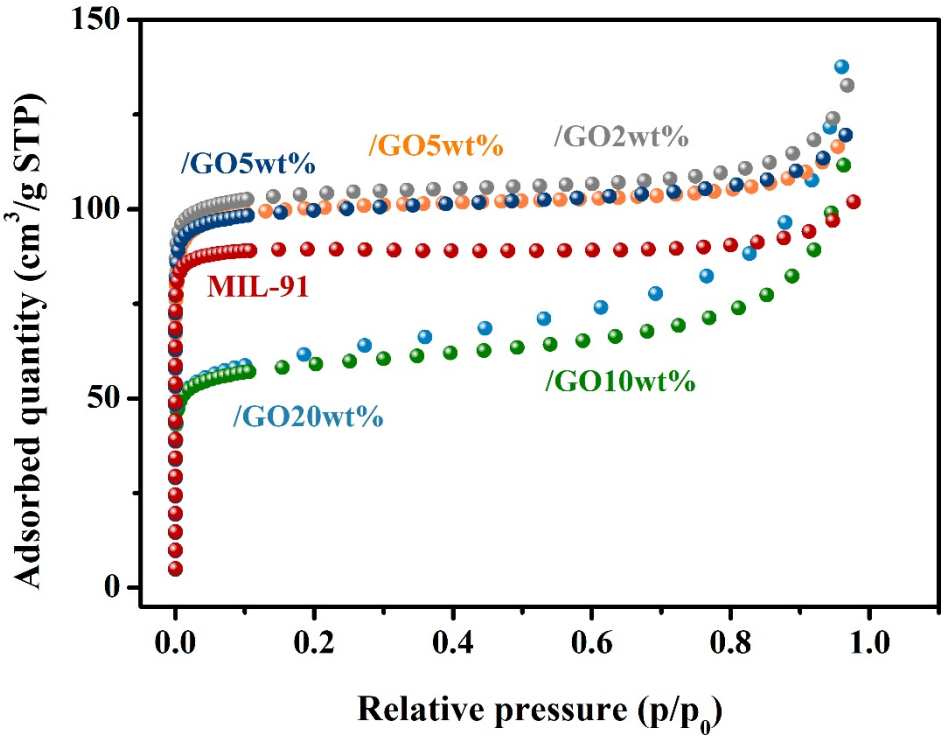

Figure 3. Nitrogen adsorption isotherms at 77 K of MIL-91(Ti) (red), MIL-91(Ti)/GO2wt% *in situ* (grey), MIL-91(Ti)/GO5wt% *in situ* (orange), MIL-91(Ti)/GO10wt% *in situ* (green), MIL-91(Ti)/GO20wt% *in situ* (blue), MIL-91(Ti)/GO5wt%post-synthesis (dark blue).

Table 1. N_2 BET surface area, external surface area, micropore area, micropore volume of MIL-91(Ti), MIL-91(Ti)/GO5wt% *in situ* and post-synthesis (T=77 K, P_0=1 atm.).

	S_{BET} (m^2/g)	S_{Ext} (m^2/g)	S_{Micro} (m^2/g)	V_{Micro} (cm^3/g)
MIL-91(Ti)	370	12	358	0.13
MIL-91(Ti)/GO5wt% *in situ*	405	25	380	0.14
MIL-91(Ti)/GO5wt% post-synthesis	385	23	362	0.14

The 5wt% GO composites were further characterized by electron microscopy. It showed that in both cases (i) MOF particles are in close contact with the GO sheets together with a few isolated bare MOF nanoparticles (Figure S8, S9) and (ii) MOF crystals exhibit a rod-like morphology with a high polydispersity in size (Figure S6.1, S10). Energy-dispersive X-ray spectroscopy (EDS) mapping shows a homogeneous distribution of titanium and phosphorus elements within the MOF crystals with similar Ti/P ratio of 0.50 and 0.48 for the *in situ* and post-synthetic samples, respectively (theoretical value : 0.5) (Figure S11).[20] Noticeably, only the EDS mapping of the *in situ* composite reveals that the GO sheets are covered by phosphorus and titanium atoms, in agreement with the Ti2p XPS spectra that shows two chemical environments (Supporting information, Figure S13). This is in line with a complexation of titanium cations on the oxygenated groups of GO and confirms that those groups act as nucleation sites for the MOF growth, as already observed for other MOF/GO systems.[15, 30-32] In addition, when the synthesis of pure MIL-91(Ti) was carried out under similar concentration conditions (30 mL water at t = 0 min and addition of 30 mL water after 6 hours, see experimental section), the resulting solid was amorphous. This

further confirms that the oxygenated groups of GO participate actively to the heterogeneous nucleation and growth of the MOF in these conditions.

SAED measurements performed on the *in situ* composite showed that the MOF growth occurs along the [010] direction, corresponding to the Ti-O-Ti corner-sharing chains of Ti octahedra (Figure S14).

As the main objective here is to design MOF/GO composites with sufficient electrical conductivity for CO_2 capture by MSA process, the study of the Csp^2 content of GO, that tailors the electron pathway, through XPS C1S spectrum is of particular interest. As illustrated by Figure S15, the C1s spectra of MIL-91(Ti)/GO5wt% *in situ* shows a peak at 284.3 eV that is not observed for the post-synthetic material. This binding energy corresponds to Csp^2, which suggests that GO was partially reduced during the synthesis (see Figure S16 and Table S4 for the XPS C1s spectrum of pure GO). It has been previously reported that GO reduction under heating is more efficient in polar solvent such as water or DMF than in air.[33] To confirm this GO reduction, pure GO sheets were placed in water under reflux overnight. As shown in Figure S17 the GO was indeed slightly reduced, as revealed by the increase of the contribution of Csp^2 compared to the initial GO together with a C/O ratio (from XPS) of 2.4 instead of 2.0 for the initial GO. Therefore, the synthetic conditions of the *in situ* composite leads to a slight reduction of GO that might affect the composites' physicochemical properties.

Electrical conductivity and dielectric properties

To use the composites in MSA process, the microwave absorption of the material must be high enough to trigger a temperature increase through energy dissipation. The interaction of microwaves with an ideal material that consists of non-interacting dipoles with one relaxation time is described

by the Debye relaxation.[14] It is usually expressed by the complex permittivity ε^* that decomposes into a real part (ε'), associated with the energy storage ability of the material and an imaginary part (ε'') which is related to the dielectric losses and the dissipation of the absorbed energy into heat. They are described according to equation (1) and (2), respectively.

$$\varepsilon' = \varepsilon_\infty + \frac{(\varepsilon_s - \varepsilon_\infty)}{1 + \omega^2\tau^2} \quad (1)$$

$$\varepsilon'' = \frac{(\varepsilon_s - \varepsilon_\infty)\omega\tau}{1 + \omega^2\tau^2} + \frac{\sigma}{\omega\varepsilon_0} \quad (2)$$

With ε_∞ the permittivity at high frequency limit, ε_s the static permittivity, ω the angular frequency, τ the relaxation time, ε_0 is the dielectric constant of free space and σ the electrical conductivity at the frequency ω.

The microwave absorption of the material, represented by ε'', depends on its polarizability and electrical conductivity. Therefore, materials suitable for the MSA process should absorb microwave (i) enough to minimize the energy penalty of the process, and (ii) not too much to avoid any microwave penetration issues through the adsorption column. To achieve this, they must exhibit a semi-conducting behavior. The electrical conductivity of the pure components and composites were measured using complex impedance spectroscopy. As shown by the very low conductivity value ($\sigma < 10^{-8}$ S.cm^{-1} at 373 K) combined with the absence of the σ_{dc} plateau (Figure 4), MIL-91(Ti) is insulating, indicating that no electronic nor ionic charges diffuse over long distances. This behavior is maintained for the post-synthesis composite whatever the GO content, while pure GO shows a semi-conducting behavior ($\sigma_{dc} = 10^{-4.8}$ S.cm^{-1}). The dilution of GO inside the insulating MOF particles seems to induce a poor recovery of the Csp^2 clusters at the sheet-to-

sheet junctions, preventing the electron hopping and tunneling of GO.[34] Alternatively, MIL-91(Ti)/GO5wt% *in situ* behaves like a semi-conducting material, with a conductivity value ($\sigma_{dc} \approx 10^{-5}$ S.cm^{-1}) converging towards that of the pure GO despite the presence of the insulating MOF as a main phase. This may be due to i) the partial reduction of GO during the synthesis and/or ii) specific MOF/GO interactions allowing to retain the electrical conductivity of pure GO. To support the first assumption, the electrical conductivity of GO previously soaked in water under reflux overnight was measured. The obtained electrical conductivity is slightly higher than that of pure GO, in agreement with a low reduction degree. It is noteworthy that this increase in value is however too small to explain the higher level of the electrical conductivity of the *in situ* composite compared to that of the post-synthesis one.

Thus, the specific electrical behavior of the *in situ* composite most probably arises from its peculiar microstructure. The formation of this composite involves a direct complexation of Ti cations on the oxygenated groups of GO, followed by the crystal growth, most probably on the sp^3 regions of the GO sheets. In addition, the reflux itself leads to the removal of oxygen atoms that are not coordinated to the MOF, leading to the creation of additional sp^2 clusters, free from any insulating MIL-91(Ti) crystals. As a consequence, the MOF particles most likely do not interfere with the electron hopping of GO that occurs between the sp^2 regions, leading to a material with similar electrical conductivity than pure GO.

The imaginary parts of the dielectric permittivities of pure MIL-91(Ti), GO and the two composites with 5wt% GO were then measured at the microwave frequency of 2.45 GHz from 20°C to 120°C with the cavity perturbation method (Supporting information). As shown in Figure S18, MIL-

91/GO5wt% *in situ* exhibits a higher value of the imaginary part (ε") compared to that of the post synthesis composite, which is consistent with the electrical conductivity results.

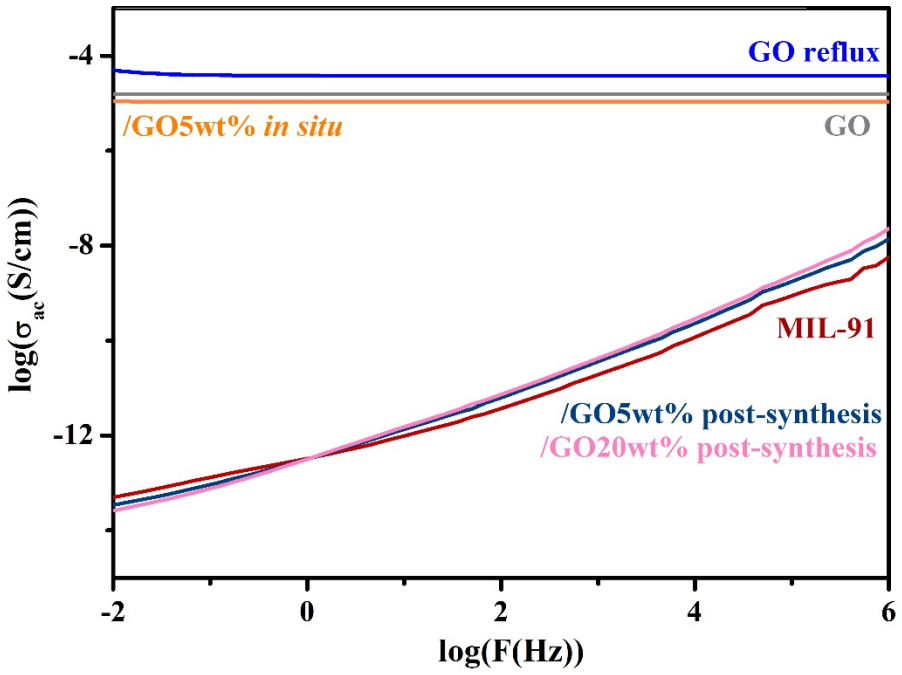

Figure 4. Real part of the conductivity as a function of the frequency recorded at 373 K for GO, GO after 16 h reflux in water, MIL-91(Ti), MIL-91(Ti)/GO5 and 20wt% post-synthesis and MIL-91(Ti)/GO5wt% *in situ*.

Breakthrough curves and CO_2 desorption under conventional and microwave heating

Considering the larger microwave absorption and suitable porosity of the MIL-91(Ti)/GO5wt% *in situ* composite, this material was selected for the CO_2 desorption under microwave irradiation tests.

First, the pure CO_2 isotherm of the composite was measured and compared to that of the pure MOF. The composite exhibits a higher CO_2 adsorption (Figure S19, Table S5), in agreement with its higher micropore area (Figure 3, Table 1). This increase of CO_2 adsorption was already observed for other MOF/GO systems and was attributed to the adsorption of CO_2 molecules not only within the MOF porosity, but also within the micropores at the MOF/GO interface.[5, 35-37]

To avoid any significant drop pressure effects inside the separation column during the desorption tests, the powder was shaped through wet granulation using 3wt% of polyvinyl butyral as the binder, yielding 1 to 2 mm size beads. As shown in Figure S19, the single CO_2 adsorption isotherms revealed a lower adsorption capacity for MIL-91/GO5wt% spheres compared to the powder, evidencing a slight pore blocking by the polymeric binder (Table S5).

The co-adsorption measurements were performed by saturating the column with a CO_2/N_2 15/85 mixture at atmospheric pressure and 30 °C. When saturation is reached, the material is filled by the gas molecules which leads to the detection of what was injected in the column *e.g* 15 % molar CO_2 and 85 % N_2. The desorption was then carried out under conventional heating and under microwave irradiation at 50 °C (Supporting information). The temperature was monitored by an infrared camera. To reach the desorption temperature, a continuous MW power of 250 W was required. As shown in Figure 5.2, CO_2 is completely desorbed after 150 seconds under irradiation, significantly faster than under conventional heating which required 240 seconds (Figure 5.1). The adsorption/desorption cycles are reproducible under both conventional heating and MW radiations, giving evidence that the desorption processes do not damage the composite and that the adsorption capacity is maintained. However, the cyclability under MW radiation will have to be investigated over more cycles in the near future to confirm the long-time stability and efficiency. Noticeably, desorption under conventional heating was also performed at 80 °C and led to a desorption time of 215 seconds, longer than what was obtained under MW radiations at 50 °C (Figure S20).

To investigate whether this faster CO_2 desorption under MSA process is specific to MIL-91(Ti)/GO *in situ* systems, composites were synthesized with a MOF exhibiting a different structure and composition (metal, linker) , namely UiO-66-btc(Zr).[38, 39] This MOF is a zirconium(IV) oxo-cluster

tri-carboxylate material with a cubic architecture delimiting two types of microporous cavities and exhibits free COOH groups suitable to interact specifically with CO_2 molecules (Figure S21).[40] Similarly to the MIL-91/GO composites, the UiO-66-btc(Zr)/GO *in situ* composite exhibited a higher microwave absorption (ε'') compared to the post-synthetic material and pure MOF (Figure S24). To reach the desorption temperature on the UiO-66-btc(Zr)/GO10wt% *in situ* composite, a MW power of 390 W was applied, higher than what was used for the MIL-91(Ti)/GO5wt% composite, in agreement with its lower MW absorption. The desorption time under microwave radiations at 50 °C is again much shorter (approximately 120 sec) compared to the desorption time under conventional heating (approximately 210 sec) at the same temperature (Figure 5.4). Therefore, it confirms that the faster CO_2 release under MW irradiation is not governed by the nature of the MOF itself but rather by the specific structure of the *in situ* composites. The good cyclability of the experiment was evidenced by the superimposition of the breakthrough curves.

These results undoubtedly confirm that MW desorption is more efficient that conventional electrical heating, even at lower desorption temperatures. The faster desorption under MW can be attributed to a higher heating rate as well as a more homogenous heating. Indeed, under conventional heating, the sides of the column are first heated, followed by a slow heat transfer from the sides to the material at the center. On the other hand, MW radiations cause a volumetric heating of the material and is thus more efficient and homogeneous on these composites. These results evidence that the use of microwave absorbing MOF/GO *in situ* materials is a promising strategy for CO_2 capture by microwave swing adsorption processes.

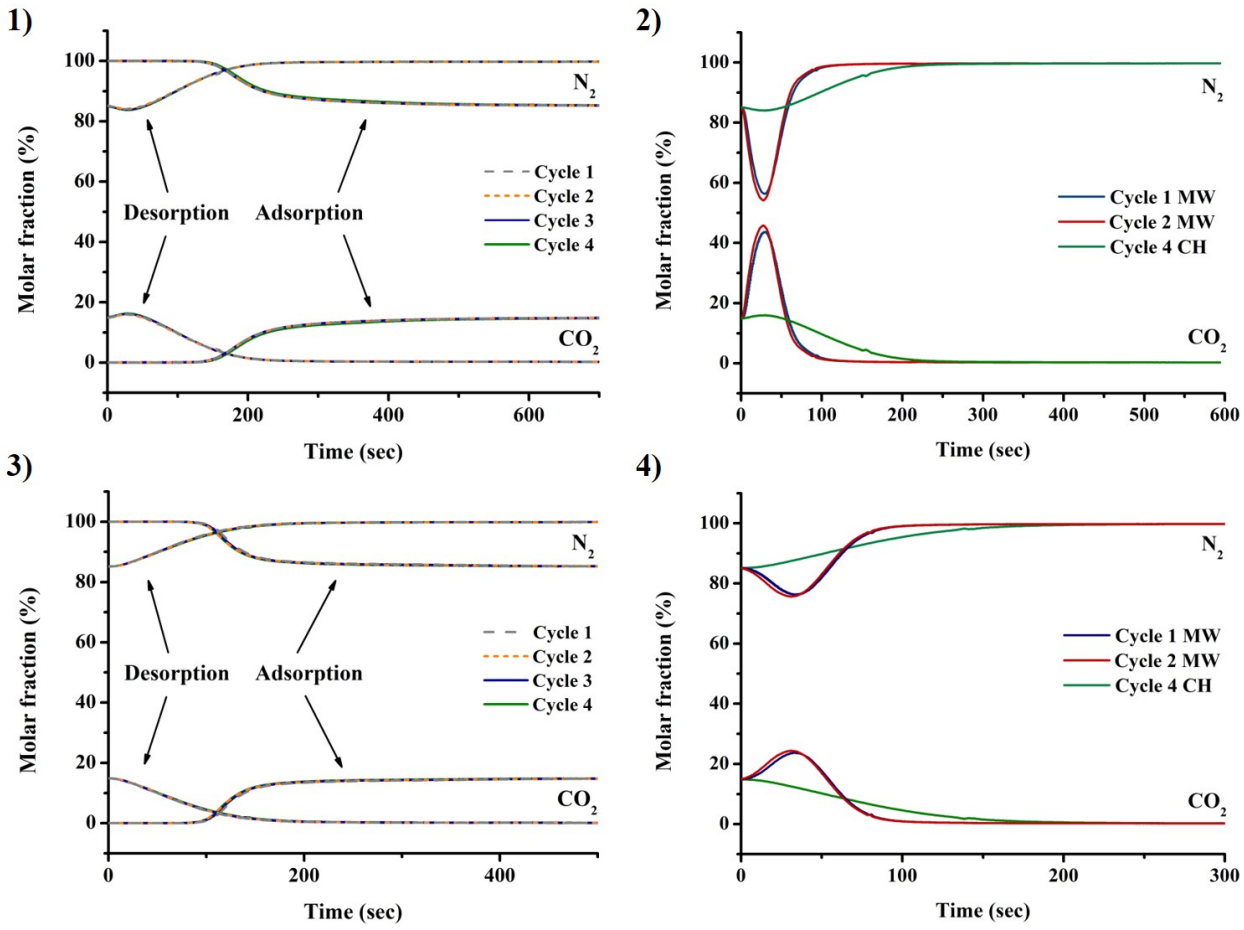

Figure 5. 1) and 3) Breakthrough adsorption curves (mixture CO_2/N_2 15/85 molar, atmospheric pressure, 30 °C) and desorption under conventional heating (CH) at 50 °C over 4 cycles. 2) and 4) Breakthrough desorption curves under MW radiation at 50 °C over 2 cycles compared with the fourth breakthrough desorption curve obtained under CH for 1) and 2) MIL-91/GO5wt% *in situ* and 3) and 4) UiO-66-btc(Zr)/GO10wt% *in situ*.

Conclusion

MOF/GO composites suitable for CO_2 capture based on the robust MIL-91(Ti) material have been prepared with different GO contents following different synthetic strategies, *in situ* or post-synthetic. We have shown that the *in situ* composite with 5wt% GO exhibits suitable electrical properties for the MSA process. Indeed, the selective growth and crystallization of the MOF over the sp^3 areas of GO induces a specific microstructure for which the insulating MOF particles do not disturb the electron hopping between the sp^2 clusters of GO. Therefore, MIL-91/GO5wt% *in*

situ exhibits a semi-conducting behavior whereas post-synthesis composites are insulating, even with relatively high GO content. Finally, MIL-91/GO5wt% *in situ* composite was evaluated for CO_2 capture with a desorption under microwave irradiation. A much faster release of CO_2 at low temperature (50 °C) under microwave irradiation compared to conventional heating was observed. Similar results were obtained with another MOF/GO *in situ* composite based on the UiO-66-btc(Zr) structure, highlighting the versatility of our strategy. It evidences the great potential of these composite materials for CO_2 capture by MSA process.

Acknowledgements

The authors would like to acknowledge the EU Research and Innovation program Horizon 2020 (H2020/2014-2020) for funding the research presented in this article under Grant Agreement No. 727619 (project Gramofon). The authors would like to acknowledge B. Alonso, A. Ortega from Graphenea S. A. (www.graphenea.com) for providing the graphene oxide. The electrical measurements were performed with the support of the Balard Plateforme d'Analyses et de Caractérisation (PAC Balard). The authors acknowledge John Brown for his help in revising the manuscript.

Declaration of Interests

The authors declare no competing interests.

References

1. Liu, X.-W.; Sun, T.-J.; Hu, J.-L.; Wang, S.-D., Composites of metal-organic frameworks and carbon-based materials: preparations, functionalities and applications. *Journal of Materials Chemistry A* **2016,** *4* (10), 3584-3616.
2. Zheng, Y.; Zheng, S.; Xue, H.; Pang, H., Metal-Organic Frameworks/Graphene-Based Materials: Preparations and Applications. *Advanced Functional Materials* **2018,** *28* (47), 1804950.
3. Muschi, M.; Serre, C., Progress and challenges of graphene oxide/metal-organic composites. *Coordination Chemistry Reviews* **2019,** *387*, 262-272.
4. Zhou, X.; Huang, W.; Liu, J.; Wang, H.; Li, Z., Quenched breathing effect, enhanced CO2 uptake and improved CO2/CH4 selectivity of MIL-53(Cr)/graphene oxide composites. *Chemical Engineering Science* **2017,** *167*, 98-104.
5. Cao, Y.; Zhao, Y.; Lv, Z.; Song, F.; Zhong, Q., Preparation and enhanced CO2 adsorption capacity of UiO-66/graphene oxide composites. *Journal of Industrial and Engineering Chemistry* **2015,** *27*, 102-107.
6. Kumar, R.; Raut, D.; Ramamurty, U.; Rao, C. N. R., Remarkable Improvement in the Mechanical Properties and CO2 Uptake of MOFs Brought About by Covalent Linking to Graphene. *Angewandte Chemie International Edition* **2016,** *55* (27), 7857-7861.
7. Jayaramulu, K.; Datta, K. K. R.; Rösler, C.; Petr, M.; Otyepka, M.; Zboril, R.; Fischer, R. A., Biomimetic Superhydrophobic/Superoleophilic Highly Fluorinated Graphene Oxide and ZIF-8 Composites for Oil–Water Separation. *Angewandte Chemie International Edition* **2016,** *55* (3), 1178-1182.
8. Trickett, C. A.; Helal, A.; Al-Maythalony, B. A.; Yamani, Z. H.; Cordova, K. E.; Yaghi, O. M., The chemistry of metal–organic frameworks for CO2 capture, regeneration and conversion. *Nature Reviews Materials* **2017,** *2* (8), 17045.
9. Adil, K.; Bhatt, P. M.; Belmabkhout, Y.; Abtab, S. M. T.; Jiang, H.; Assen, A. H.; Mallick, A.; Cadiau, A.; Aqil, J.; Eddaoudi, M., Valuing Metal–Organic Frameworks for Postcombustion Carbon Capture: A Benchmark Study for Evaluating Physical Adsorbents. *Advanced Materials* **2017,** *29* (39), 1702953.
10. Chronopoulos, T.; Fernandez-Diez, Y.; Maroto-Valer, M. M.; Ocone, R.; Reay, D. A., CO2 desorption via microwave heating for post-combustion carbon capture. *Microporous and Mesoporous Materials* **2014,** *197*, 288-290.
11. Lee, E. J.; Bae, J.; Choi, K. M.; Jeong, N. C., Exploiting Microwave Chemistry for Activation of Metal–Organic Frameworks. *ACS Applied Materials & Interfaces* **2019,** *11* (38), 35155-35161.
12. Xie, L. S.; Skorupskii, G.; Dincă, M., Electrically Conductive Metal–Organic Frameworks. *Chemical Reviews* **2020**.
13. Sun, L.; Campbell, M. G.; Dincă, M., Electrically Conductive Porous Metal–Organic Frameworks. *Angewandte Chemie International Edition* **2016,** *55* (11), 3566-3579.
14. Quan, B.; Liang, X.; Ji, G.; Cheng, Y.; Liu, W.; Ma, J.; Zhang, Y.; Li, D.; Xu, G., Dielectric polarization in electromagnetic wave absorption: Review and perspective. *Journal of Alloys and Compounds* **2017,** *728*, 1065-1075.
15. Petit, C.; Bandosz, T. J., Engineering the surface of a new class of adsorbents: Metal–organic framework/graphite oxide composites. *Journal of colloid and interface science* **2015,** *447*, 139-151.

16. Qiu, X.; Wang, X.; Li, Y., Controlled growth of dense and ordered metal-organic framework nanoparticles on graphene oxide. *Chemical Communications* **2015,** *51* (18), 3874-3877.
17. Kumar, R.; Jayaramulu, K.; Maji, T. K.; Rao, C. N. R., Hybrid nanocomposites of ZIF-8 with graphene oxide exhibiting tunable morphology, significant CO2 uptake and other novel properties. *Chemical Communications* **2013,** *49* (43), 4947-4949.
18. Liang, R.; Shen, L.; Jing, F.; Qin, N.; Wu, L., Preparation of MIL-53(Fe)-Reduced Graphene Oxide Nanocomposites by a Simple Self-Assembly Strategy for Increasing Interfacial Contact: Efficient Visible-Light Photocatalysts. *ACS Applied Materials & Interfaces* **2015,** *7* (18), 9507-9515.
19. Muschi, M.; Lalitha, A.; Sene, S.; Aureau, D.; Fregnaux, M.; Esteve, I.; Rivier, L.; Ramsahye, N.; Devautour-Vinot, S.; Sicard, C.; Menguy, N.; Serre, C.; Maurin, G.; Steunou, N., Formation of a Single-Crystal Aluminum-Based MOF Nanowire with Graphene Oxide Nanoscrolls as Structure-Directing Agents. *Angewandte Chemie International Edition* **2020,** *59* (26), 10353-10358.
20. Benoit, V.; Pillai, R. S.; Orsi, A.; Normand, P.; Jobic, H.; Nouar, F.; Billemont, P.; Bloch, E.; Bourrelly, S.; Devic, T.; Wright, P. A.; de Weireld, G.; Serre, C.; Maurin, G.; Llewellyn, P. L., MIL-91(Ti), a small pore metal-organic framework which fulfils several criteria: an upscaled green synthesis, excellent water stability, high CO2 selectivity and fast CO2 transport. *Journal of Materials Chemistry A* **2016,** *4* (4), 1383-1389.
21. Serre, C.; Groves, J. A.; Lightfoot, P.; Slawin, A. M. Z.; Wright, P. A.; Stock, N.; Bein, T.; Haouas, M.; Taulelle, F.; Férey, G., Synthesis, Structure and Properties of Related Microporous N,N‘-Piperazinebismethylenephosphonates of Aluminum and Titanium. *Chemistry of Materials* **2006,** *18* (6), 1451-1457.
22. Hu, Y.; Wei, J.; Liang, Y.; Zhang, H.; Zhang, X.; Shen, W.; Wang, H., Zeolitic Imidazolate Framework/Graphene Oxide Hybrid Nanosheets as Seeds for the Growth of Ultrathin Molecular Sieving Membranes. *Angewandte Chemie International Edition* **2016,** *55* (6), 2048-2052.
23. Travlou, N. A.; Singh, K.; Rodriguez-Castellon, E.; Bandosz, T. J., Cu-BTC MOF-graphene-based hybrid materials as low concentration ammonia sensors. *Journal of Materials Chemistry A* **2015,** *3* (21), 11417-11429.
24. Petit, C.; Bandosz, T. J., Synthesis, Characterization, and Ammonia Adsorption Properties of Mesoporous Metal–Organic Framework (MIL(Fe))–Graphite Oxide Composites: Exploring the Limits of Materials Fabrication. *Advanced Functional Materials* **2011,** *21* (11), 2108-2117.
25. Liu, S.; Sun, L.; Xu, F.; Zhang, J.; Jiao, C.; Li, F.; Li, Z.; Wang, S.; Wang, Z.; Jiang, X.; Zhou, H.; Yang, L.; Schick, C., Nanosized Cu-MOFs induced by graphene oxide and enhanced gas storage capacity. *Energy & Environmental Science* **2013,** *6* (3), 818-823.
26. Shen, Y.; Li, Z.; Wang, L.; Ye, Y.; Liu, Q.; Ma, X.; Chen, Q.; Zhang, Z.; Xiang, S., Cobalt-citrate framework armored with graphene oxide exhibiting improved thermal stability and selectivity for biogas decarburization. *Journal of Materials Chemistry A* **2015,** *3* (2), 593-599.
27. Zhou, X.; Huang, W.; Shi, J.; Zhao, Z.; Xia, Q.; Li, Y.; Wang, H.; Li, Z., A novel MOF/graphene oxide composite GrO@MIL-101 with high adsorption capacity for acetone. *Journal of Materials Chemistry A* **2014,** *2* (13), 4722-4730.
28. Zhou, Y.; Mao, Z.; Wang, W.; Yang, Z.; Liu, X., In-Situ Fabrication of Graphene Oxide Hybrid Ni-Based Metal–Organic Framework (Ni–MOFs@GO) with Ultrahigh Capacitance as Electrochemical Pseudocapacitor Materials. *ACS Applied Materials & Interfaces* **2016,** *8* (42), 28904-28916.

29. Liu, N.; Huang, W.; Zhang, X.; Tang, L.; Wang, L.; Wang, Y.; Wu, M., Ultrathin graphene oxide encapsulated in uniform MIL-88A(Fe) for enhanced visible light-driven photodegradation of RhB. *Applied Catalysis B: Environmental* **2018,** *221*, 119-128.
30. Jahan, M.; Liu, Z.; Loh, K. P., A Graphene Oxide and Copper-Centered Metal Organic Framework Composite as a Tri-Functional Catalyst for HER, OER, and ORR. *Advanced Functional Materials* **2013,** *23* (43), 5363-5372.
31. Yang, L.; Tang, B.; Wu, P., Metal–organic framework–graphene oxide composites: a facile method to highly improve the proton conductivity of PEMs operated under low humidity. *Journal of Materials Chemistry A* **2015,** *3* (31), 15838-15842.
32. Wei, J.; Hu, Y.; Liang, Y.; Kong, B.; Zhang, J.; Song, J.; Bao, Q.; Simon, G. P.; Jiang, S. P.; Wang, H., Nitrogen-Doped Nanoporous Carbon/Graphene Nano-Sandwiches: Synthesis and Application for Efficient Oxygen Reduction. *Advanced Functional Materials* **2015,** *25* (36), 5768-5777.
33. Lin, Z.; Yao, Y.; Li, Z.; Liu, Y.; Li, Z.; Wong, C.-P., Solvent-Assisted Thermal Reduction of Graphite Oxide. *The Journal of Physical Chemistry C* **2010,** *114* (35), 14819-14825.
34. Mattevi, C.; Eda, G.; Agnoli, S.; Miller, S.; Mkhoyan, K. A.; Celik, O.; Mastrogiovanni, D.; Granozzi, G.; Garfunkel, E.; Chhowalla, M., Evolution of Electrical, Chemical, and Structural Properties of Transparent and Conducting Chemically Derived Graphene Thin Films. *Advanced Functional Materials* **2009,** *19* (16), 2577-2583.
35. Szczęśniak, B.; Choma, J.; Jaroniec, M., Gas adsorption properties of hybrid graphene-MOF materials. *Journal of colloid and interface science* **2018,** *514*, 801-813.
36. Chen, B.; Zhu, Y.; Xia, Y., Controlled in situ synthesis of graphene oxide/zeolitic imidazolate framework composites with enhanced CO2 uptake capacity. *RSC Advances* **2015,** *5* (39), 30464-30471.
37. Li, W.; Chuah, C. Y.; Yang, Y.; Bae, T.-H., Nanocomposites formed by in situ growth of NiDOBDC nanoparticles on graphene oxide sheets for enhanced CO2 and H2 storage. *Microporous and Mesoporous Materials* **2018,** *265*, 35-42.
38. Biswas, S.; Zhang, J.; Li, Z.; Liu, Y.-Y.; Grzywa, M.; Sun, L.; Volkmer, D.; Van Der Voort, P., Enhanced selectivity of CO2 over CH4 in sulphonate-, carboxylate- and iodo-functionalized UiO-66 frameworks. *Dalton Transactions* **2013,** *42* (13), 4730-4737.
39. Ragon, F.; Campo, B.; Yang, Q.; Martineau, C.; Wiersum, A. D.; Lago, A.; Guillerm, V.; Hemsley, C.; Eubank, J. F.; Vishnuvarthan, M.; Taulelle, F.; Horcajada, P.; Vimont, A.; Llewellyn, P. L.; Daturi, M.; Devautour-Vinot, S.; Maurin, G.; Serre, C.; Devic, T.; Clet, G., Acid-functionalized UiO-66(Zr) MOFs and their evolution after intra-framework cross-linking: structural features and sorption properties. *Journal of Materials Chemistry A* **2015,** *3* (7), 3294-3309.
40. Biswas, S.; Van Der Voort, P., A General Strategy for the Synthesis of Functionalised UiO-66 Frameworks: Characterisation, Stability and CO2 Adsorption Properties. *European Journal of Inorganic Chemistry* **2013,** *2013* (12), 2154-2160.